

PAPER

Polymer-based doping control for performance enhancement of wet-processed short-channel CNTFETs

To cite this article: Martin Hartmann *et al* 2018 *Nanotechnology* **29** 035203

View the [article online](#) for updates and enhancements.

Related content

- [Length separation of single-walled carbon nanotubes and its impact on structural and electrical properties of wafer-level fabricated carbon nanotube–field-effect transistors](#)
Simon Böttger, Sascha Hermann, Stefan E Schulz *et al.*
- [Carbon nanotube thin film transistors based on aerosol methods](#)
Marina Y Zavodchikova, Tero Kulmala, Albert G Nasibulin *et al.*
- [Flexible diodes for radio frequency \(RF\) electronics: a materials perspective](#)
James Semple, Dimitra G Georgiadou, Gwenhivir Wyatt-Moon *et al.*

Polymer-based doping control for performance enhancement of wet-processed short-channel CNTFETs

Martin Hartmann^{1,2,6} , René Schubel^{2,3}, Martin Claus^{2,4}, Rainer Jordan^{2,3}, Stefan E Schulz^{1,2,5} and Sascha Hermann^{1,2,5}

¹ Technische Universität Chemnitz, Center for Microtechnologies, D-09107 Chemnitz, Germany

² Center for Advancing Electronics Dresden (cfaed), D-01062 Dresden, Germany

³ Technische Universität Dresden, Chair of Macromolecular Chemistry, D-01069 Dresden, Germany

⁴ Technische Universität Dresden, Chair for Electron Devices and Integrated Circuits, D-01069 Dresden, Germany

⁵ Fraunhofer Research Institute for Electronic Nano Systems (ENAS), D-09126 Chemnitz, Germany

E-mail: martin.hartmann@zfm.tu-chemnitz.de, rene.schubel@tu-dresden.de, martin.claus@tu-dresden.de, rainer.jordan@tu-dresden.de, Stefan.Schulz@enas.fraunhofer.de and sascha.hermann@zfm.tu-chemnitz.de

Received 15 September 2017, revised 13 October 2017

Accepted for publication 27 November 2017

Published 18 December 2017



CrossMark

Abstract

The electrical transport properties of short-channel transistors based on single-walled carbon nanotubes (CNT) are significantly affected by bundling along with solution processing. We report that especially high off currents of CNT transistors are not only related to the incorporation of metallic CNTs but also to the incorporation of CNT bundles. By applying device passivation with poly(4-vinylpyridine), the impact of CNT bundling on the device performance can be strongly reduced due to increased gate efficiency as well as reduced oxygen and water-induced p-type doping, boosting essential field-effect transistor performance parameters by several orders of magnitude. Moreover, this passivation approach allows the hysteresis and threshold voltage of CNT transistors to be tuned.

Supplementary material for this article is available [online](#)

Keywords: carbon nanotubes, field-effect transistor, CNT bundling, solution-processed, passivation, doping

(Some figures may appear in colour only in the online journal)

1. Introduction

One rising star in flexible electronics, analog high-frequency (HF) electronics, and digital electronics is the single-walled carbon nanotube field-effect transistor (CNTFET). Very recently, a breakthrough in analog HF FETs was made when a transit frequency as well as a maximum oscillation frequency of 70 GHz [1] was demonstrated. The major advantages of CNTFETs are their high current density and high intrinsic mobility [2] while having a very thin channel thickness. They have the potential to be utilized in highly

linear HF devices due to the one-dimensional nature of the single-walled carbon nanotubes (CNTs) [3–5]. This may enable a new class of highly energy-efficient analog HF devices and circuits that can outperform CMOS-based devices and circuits [6, 7]. Nevertheless, many challenges remain on the way towards industrial scalable, cost-efficient and reliable processes. In the scientific community, various integration techniques have been suggested. Among the suggested techniques, dispersion-based approaches such as spray coating [8], spin-on deposition [9], printing techniques [10], Langmuir–Blodgett methods [1], and dielectrophoresis (DEP) [11–14] appear very promising, since CNT material with a purity higher than 99% is now easily available due to

⁶ Author to whom any correspondence should be addressed.

breakthroughs in polymer-based sorting techniques [14–19]. However, in the previously suggested integration techniques, special attention needs to be paid to the morphology of the transistor channel, since CNTs agglomerate bundle due to van der Waals interaction. This occurs either in the dispersion, during the rinsing, or the liquid/dry phase transition. The resulting CNT bundles negatively affect the final FET performance, resulting in low on–off current ratios [20, 21]. For analog HF applications, the situation becomes even more critical, since the mandatory high drive currents can only be obtained by dense CNT assemblies [1, 22, 23], which inevitably increases the risk of CNT agglomeration. In those cases, high density is accompanied by low on–off ratios due to metallic CNTs and CNT bundles. This issue becomes apparent in the work of Cao *et al* [1], who reported 70 GHz transistors but only on–off ratios up to 2000. Furthermore, the direct environment of the CNTs has a strong impact on their electrical properties [24]. Charges and charge traps in close proximity to the tubes can tremendously perturb the ideal device performance. Such charges and charge traps can occur, among other places, at the interface between the tubes and the oxide substrate, inside the oxide, or in adjacent residual particles [25, 26]. As a result, hysteresis can be observed in the FET transfer characteristics measured during a forward sweep and subsequent backward sweep of the gate voltage and in a drifting bias point over time. In addition, the AC performance is deteriorated due to the inertia of the capacitive-coupled charges/traps and the additional power needed to charge/discharge them [27]. Since CNTs are sensitive to different molecules in the gas or vapor phase, the presence of oxygen in particular significantly affects CNTFETs operating at ambient conditions [24]. Collins *et al* and other groups [28–30] reported that an oxygen environment leads to a change in the electrical resistance, the local density of states, and to a p-type doping. In the literature, doping is usually mentioned as being extrinsically introduced to achieve unipolar n-type devices with increased on currents, for example, doping with alkali metals [31] or amine-rich polymers [32]. To achieve device performances that are insensitive to changes in the local environment and to exploit the intrinsic CNT properties without ambient influences, the CNTs must be passivated with an adequate capping layer. Different materials have been deployed as passivation, like silicon oxide [33, 34], hydrogen silsesquioxane [35], silicon nitride [36, 37], and polymers like polymethylmethacrylate (PMMA) [38–40], poly (sodium 4-styrenesulfonate) [21, 41], polymerized fluorocarbons [42, 43], and poly(vinylphenol)/poly (methyl silsesquioxane) blends [43].

In the present study, we investigated an alternative, performance enhancing method of passivating CNTFET devices on the basis of Poly(4-vinylpyridine) (PVP), which is a neutral polymer known for debundling CNTs in aqueous solution via photografting [44]. Within the scope of a scalable technological process flow, we employed two different approaches to integrate a PVP passivation layer and studied its influence on the electrical properties of dispersion-based short-channel CNTFET arrays. Furthermore, we present a

strategy to overcome the negative impact of doping in combination with bundled CNTs on the FET performance.

2. Experimental section

2.1. Sample preparation

CNTFETs were fabricated on 150 mm diameter silicon wafers covered with 2 μm thick thermally grown SiO_2 . A single damascene process was used to form planar gate electrodes. On top of the 200 nm thick AlSiTi gate metallization, a 50 nm thick SiO_2 gate dielectric layer was deposited via chemical vapor deposition. The source and drain electrodes were formed by a conventional lift-off procedure using a thin aluminum adhesion layer and 20 nm thick palladium layer. Palladium was chosen due to its good wetting behavior on the CNTs [45, 46] as well as its work function [45, 47]. The devices for the PVP spin-on and the polymerization experiments were fabricated with a channel length of (700 ± 80) nm and (760 ± 40) nm, respectively. The CNTs were integrated via DEP, followed by a water-rinsing step. For the DEP, an AC signal with a frequency of 10 MHz and a peak-to-peak amplitude of 1 V was applied for 20 s. A commercially available single-walled CNT dispersion from NanoIntegris (IsoNanotubes-S [48]) with a purity of 99.9% semiconducting nanotubes was used. The dispersion was further diluted with a sodium dodecyl sulfate (SDS)/DI-water mixture (1 wt% SDS in DI-water) with a ratio of 1:9. To remove the remaining surfactant molecules as well as to strengthen the contacts between the CNTs and the metal electrodes, the FETs were annealed in vacuum at 558 K for 45 min. As the final step, a 10 nm thick palladium top contact was formed on the source and drain electrodes via e-beam lithography patterned PMMA resist, and an additional lift-off process defined the final channel length. Two different passivation methods were investigated and thus two sample batches were fabricated. The channel lengths of the FETs were (390 ± 35) nm for the spin-on passivation experiments and (650 ± 20) nm for the *in situ* polymerization experiments. To passivate the CNTFETs via a spin-on process with PVP, the polymer was solved in isopropanol and spin-coated onto the devices for 10 s at 1000 rpm. The CNTFETs were characterized electrically as well as by atomic force microscopy (AFM) and Raman spectroscopy prior to and after the spin-on process.

The passivation of the CNTFETs via *in situ* polymerization of vinylpyridine was performed stepwise to trace the polymerization process and its effect on the CNTFETs. The monomer solution of vinylpyridine was degassed by nitrogen for at least 15 min. Afterwards, the CNTFET sample was placed in the monomer solution and a self-initiated photografting and photopolymerization process was initiated via a UV lamp [49]. In total, the samples were polymerized for 120 min to 150 min, leading to a polymer thickness of (10 ± 2) nm (for more information on the polymer layer morphology, see figure S3 is available online at stacks.iop.org/NANO/29/035203/mmedia of the supplementary information).

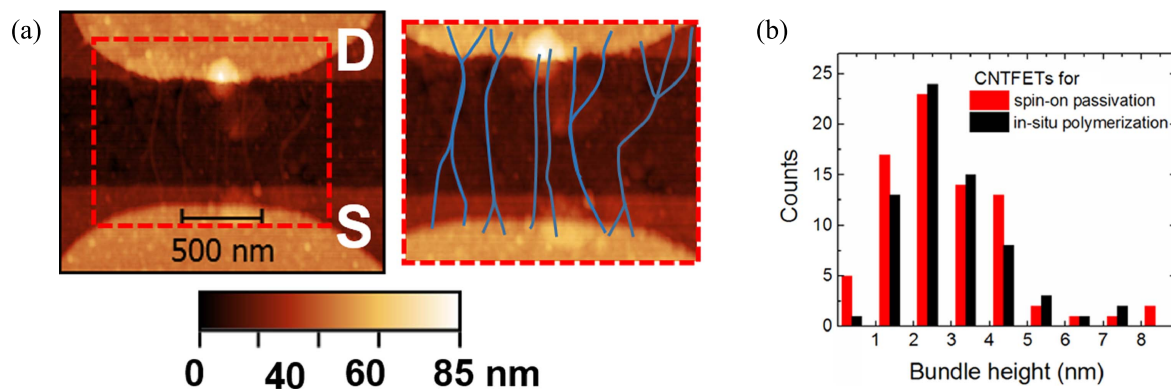


Figure 1. (a) AFM topography image of a CNTFET: the source (S) and drain (D) electrodes are on the bottom and on the top, respectively; the lines between them are the CNTs, fully embedded in metal at their ends. (b) Frequency distribution of the CNT bundle heights extracted from AFM topography images. The red and black bars correspond to the sample batch for the spin-on passivation and *in situ* polymerization experiments, respectively.

2.2. Characterization

Selected CNTFETs were characterized by an Agilent 5600LS atomic force microscope in intermittent contact mode before the passivation to analyze the structure of the device and the amount of the incorporated CNTs as well as their alignment. An example CNTFET before polymerization is shown in figure 1(a). The electrical characteristics were measured using a dual-channel Keithley 2636B source meter combined with a probe station from SUSS MicroTec GmbH. All electrical measurements were done at ambient conditions. The transfer characteristics were measured by a successive forward and backward staircase voltage sweep and by an pulsed voltage sweep [27, 50]. The later can be used under certain conditions to measure trap-unaffected figures of merit (FOMs), while a staircase voltage sweep leads to trap-affected transistor characteristics. From such transfer characteristics measured by the pulsed method, several FOMs were extracted. The off currents were extracted from pulsed measurements by finding the smallest value of the current. In order to get threshold voltages independent of the on currents, a proper gate overdrive voltage was used to extract the I_{on} . The threshold voltages were extracted by fitting a linear function around the point of maximal slope (absolute value) of the transfer characteristics. To quantify the impact of the charge traps, the width of the hysteresis of a successively forward and backward staircase voltage sweep was extracted in the middle of the maximal current difference between the forward and the backward sweep.

2.3. Simulations

The multiscale simulation framework described by Claus *et al* [4, 51] was employed to study the impact of CNT proximity and water-induced doping in CNT bundles. The carrier transport along a single CNT in a bundle is described by an augmented drift-diffusion model which captures tunneling effects at the metal-CNT junctions by means of the Wentzel-Kramers-Brillouin approximation. The electrostatic interaction between closely packed CNTs is considered via symmetry lines to the left and to the right of the simulated CNT,

where the distance between the symmetry lines is identical to the assumed distance between the centers of neighboring tubes. Water-induced doping is assumed in all simulations. Depending on the degree of polymerization and thus on the degree of water displacement, different doping concentrations are considered, ranging from 0 up to $5 \times 10^5 \text{ cm}^{-1}$ for a CNT which is significantly affected by water. The trap-like character of water-induced doping is not considered in the simulations since the simulations are compared to trap unaffected electrical measurements. Details of the simulated device architecture do not change the qualitative impact of the proximity effect due to the doping studied in this article. Consequently, for simplicity, the device architecture has been set to a global back gate with a channel length of 50 nm, an oxide thickness of 20 nm and a dielectric constant of 4. The Schottky barrier height was set to 0.1 eV. The mobility model was adjusted to fit BTE results [4].

3. Results and discussion

Before the passivation and polymerization experiments, the CNTFET channel morphology was investigated via AFM measurements after dielectrophoretic CNT integration. Figure 1(a) shows an example of filigree CNTs and CNT bundles bridging the gap between the sources and drain metal electrodes. As an indication of bundle formation, the thickness distribution of individual CNTs or CNT bundles was analyzed from 10 devices by evaluating their height. The two device batches used in this study for the spin-on and the *in situ* polymerization passivation experiments showed very similar height distributions of $(2.9 \pm 1.6) \text{ nm}$ and $(3.0 \pm 1.5) \text{ nm}$ as visualized in figure 1(b). Since individual CNTs have a diameter of 1.2–1.7 nm, we conclude that small bundles are present. Additionally, we analyzed the amount of CNTs or CNT bundles per FET. Our results indicate that around (16 ± 10) CNTs or CNT bundles were integrated per device. Moreover, the topography analysis indicates that individual tubes or small bundles tend to aggregate in the FET's channel, forming Y-like CNT-bundle structures close to the metal

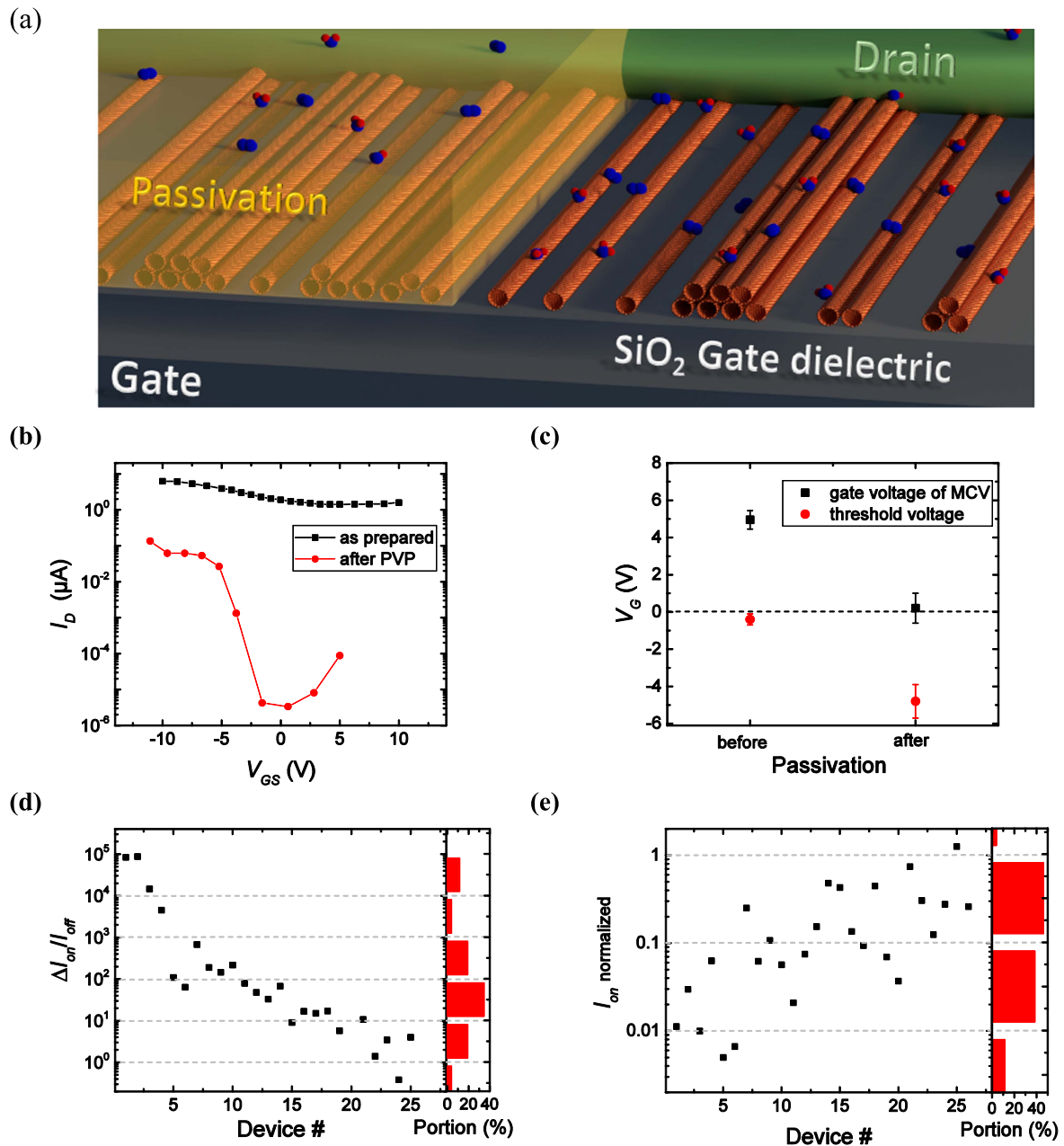


Figure 2. (a) Schematic image of a CNTFET illustrating on the left side CNTs passivated against water and oxygen molecules and on the right side exposed CNTs. (b) Comparison of the transfer characteristics of a CNTFET before and after PVP coating; measurements were performed in the pulsed mode at $-0.1 V_{DS}$. (c) The threshold voltage and the gate voltage at minimum I_{DS} (MCV) for one CNTFET before and after PVP coating. (b) and (c) show measurements on the same FET. (d) and (e) show the statistical deviation for 26 FETs. The devices were sorted ascending with respect to their off current I_{off} after PVP coating. (d) Difference between the I_{on}/I_{off} ratio before and after PVP coating. (e) Change in the on current I_{on} for the same devices. The I_{on} after passivation was normalized to the original I_{on} .

electrodes. This indicates bundle formation during the deionized (DI) water rinsing at the end of the DEP process.

To investigate the impact of CNT bundles on the CNTFET properties, we measured the electrical characteristics before and after the spin-on PVP passivation of the devices. The initial electrical characterization confirms the presence of CNT bundles. This structural configuration deteriorates the electronic properties of the FET, mainly due to mutual screening [52] strongly reducing the coupling between the gate and the tubes within the bundle. Thus, the effective gate-induced electric field experienced by a CNT

depends on the position of the tube in the bundle. Larger gate voltages are therefore required to switch all the individual tubes in the bundle. Consequently, CNTFETs with CNT bundles generally show smaller on/off-current (I_{on}/I_{off}) ratios and increased subthreshold swings.

The first set of experiments investigated the impact of applying PVP coating via a simple spin-on process on the characteristics of the CNTFETs. A schematic illustration of a passivated and not passivated device can be seen in figures 2(a) and (b) shows the transfer characteristics of an example device before and after passivation. Before

passivation, the transfer characteristics indicate a strong metallic-like behavior, since the device cannot be switched off. Upon spin-on passivation, the total drain current I_D decreased by more than one order of magnitude, while the off current I_{off} decreased by around six orders of magnitude. As a result, the total on-off current ratio (I_{on}/I_{off}) increased significantly. Furthermore, figure 2(c) shows that the gate voltage at the minimum current value (MCV) as well as the threshold voltage both shift towards higher negative gate voltages. The ambipolarity of the devices also appears to be more pronounced. In order to confirm a statistical significance for this result, 26 devices were studied before and after spin-on passivation. The changes in I_{on}/I_{off} and I_{on} are shown in figures 2(d) and (e), respectively. In general, 92% of all investigated FETs revealed an increase in I_{on}/I_{off} , and 70% of the FETs increased by even more than one order of magnitude. In 15% of the devices, the I_{on}/I_{off} increased considerably by more than three orders of magnitude. Thus, the metallic-like behavior of the CNTFETs could be converted to semiconductor-like behavior. However, there is a variation in the I_{on}/I_{off} over several orders of magnitude among the samples, which is mainly due to a variation in the bundle size and in the number of parasitic metallic tubes. The gate leakage currents did not change upon passivation and were around the detection limit of our source-measuring unit.

As described above, CNT bundles in an FET channel lead to adverse performance of the device due to the complex influences on all CNTs. The improvements in the FET characteristics upon spin-coating with PVP can partly be explained by better gate coupling due to a higher permittivity of the dielectric environment around the CNTs and the CNT bundles. Through CV measurements, the permittivity of PVP was determined to be $\epsilon_r^{PVP} = (2.9 \pm 0.6)$, which is three times higher than air (see supplementary information figure S2). This leads to more efficient coupling of the electric gate field to the ensemble of CNTs in the bundles, a reduced subthreshold swing, and consequently, a narrower gate range for switching the FETs. Figure 2(b) indicates that after passivation, the subthreshold swing is reduced more than an order of magnitude, giving a value of up to 950 mV/decade, which can be expected for multitube devices with a 50 nm thick SiO_2 gate oxide [53]. Hence the gate efficiency parameter α ($\alpha = k_B T e^{-1} \ln(10) S^{-1}$) [54, 55], defined as the deviation of the actual subthreshold swing S from the ideal one at room temperature, increased by a factor of 18. This demonstrates that the gate efficiency of the CNTFETs can be strongly increased via PVP spin-on passivation.

Before and after passivation, the devices retained ambipolar FET characteristics, with a dominating p-type branch due to palladium contacts. Upon passivation, the current in the hole injection region decreased, while the electron injection current increased relative to the hole current. Additionally, the threshold voltage shifted towards negative gate voltages, and the gate voltage at the MCV decreased to an absolute value of almost zero V_{GS} . Hence the spin-on passivation reduced the p-type doping of the CNTFET channel region. The typical p-type doping of the CNTFETs is already

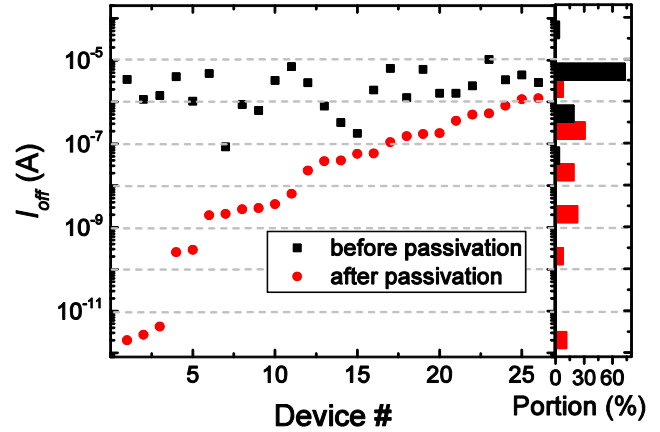


Figure 3. Comparison of the I_{off} of the CNTFETs before and after spin-on passivation.

known, as our transistors are stored under ambient conditions and oxygen is known to act as a p-type dopant for CNTs [24]. Thus, the PVP spin-on passivation successfully reduces the impact of oxygen-induced doping on the devices.

The reduction of the p-type doping also effects I_{off} . Due to the oxygen-induced doping, the CNTs in the channel are already conductive at zero V_{GS} . To switch off the transistors, 5 V is applied at the gate to counterbalance the oxygen-induced doping. While this voltage is sufficiently large enough to switch off CNTs with a good gate coupling, CNTs in tube bundles, which are affected by intertube screening, are less affected by the gate-voltage-induced electric field and are still conductive, leading to a relatively high I_{off} . In the case of passivated CNTs, the oxygen-induced doping is reduced significantly, and even the tubes with worse gate control are switched off at 5 V_{GS} , leading to a very low I_{off} . Therefore, the I_{on}/I_{off} ratio of the passivated CNTFETs significantly increases, even though the reduction in oxygen-induced doping slightly lowers I_{on} as well. In this way, the CNTFETs were converted to enhancement mode devices. This effect is more pronounced for devices without metallic tubes and with small bundle diameters. Due to an inhomogeneity in the CNT assembly, the devices show a distribution of FET properties leading to differing values for the change in I_{on}/I_{off} (figure 2(d)). The few FETs which showed almost no change in I_{on}/I_{off} are perturbed by metallic tubes dominating the device performance. However, in general, reduced p-type doping results in increased I_{on}/I_{off} due to the conversion of the FETs to enhancement mode devices. Consequently, this study suggests that the I_{off} in wet-processed CNTFETs is not only due to metallic impurities. Although it has been reported in literature that certain FOM like hysteresis width and the subthreshold swing are improving upon annealing similar to our results [40, 42], an increase over several orders of magnitude of the I_{on}/I_{off} of short channel multitube CNTFETs has not been shown yet.

The analysis of the off current before and after passivation for the different devices allows the contributions from doping and metallic CNTs to be differentiated. Figure 3 shows that the I_{off} after passivation is independent of the I_{off}

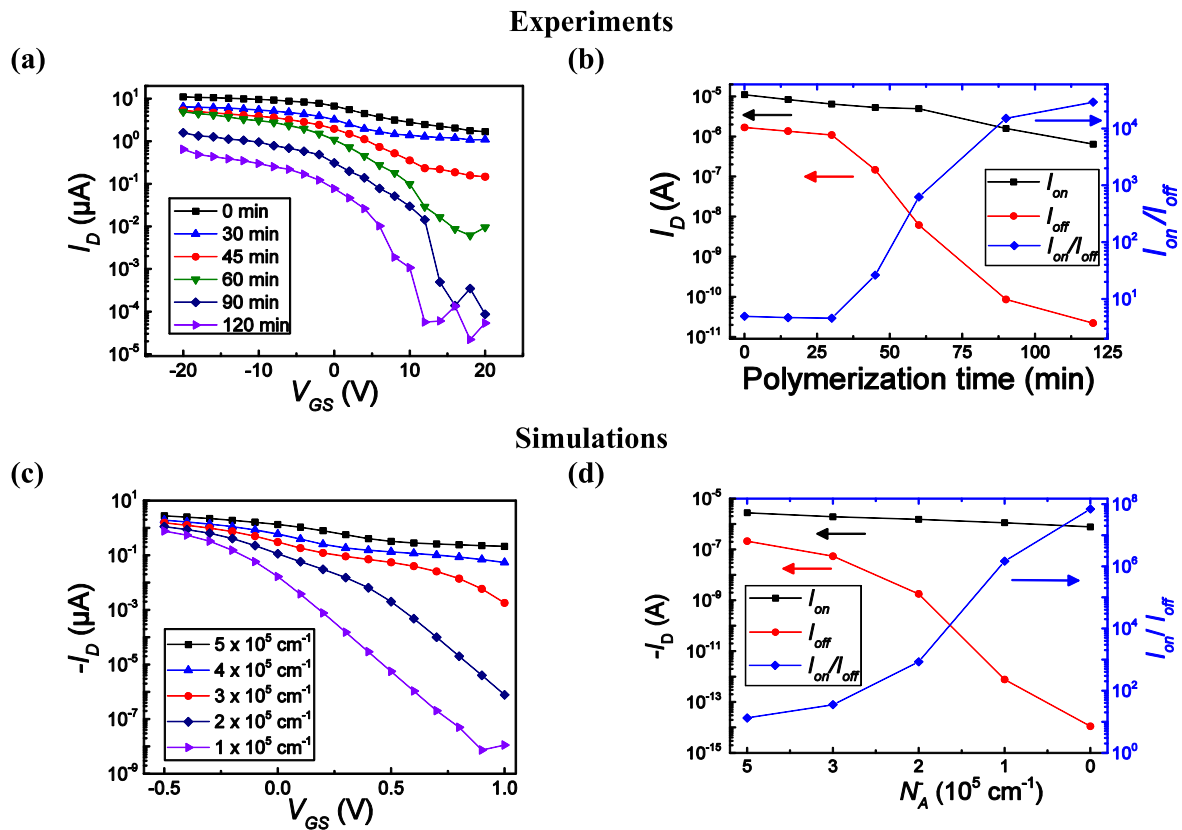


Figure 4. (a) Transfer characteristics of one CNTFET after each polymerization step measured using the pulse method and a source-to-drain voltage of 0.1 V. (b) The trace of the on and off currents as well as the corresponding I_{on}/I_{off} ratio. (c) Simulated transfer characteristics of a CNTFET with bundled and individual CNTs upon different doping concentrations. (d) Change in the on and off current as well as the I_{on}/I_{off} ratio.

before passivation. Therefore, before spin-on passivation, no conclusions can be made based on the I_{off} alone as to whether the I_{off} contribution comes from metallic CNTs or doped CNT bundles. Since the passivation minimizes the effect of CNT bundles, the I_{off} after passivation will be dominated by metallic tubes. As seen in figure 3, our results indicate that a high off current in wet processed, multi-tube short channel CNTFETs is due to both bundled CNTs and metallic tubes in the FET channel. The contribution of the CNT bundles to the whole off current can be strongly reduced via PVP spin-on passivation.

To adjust FET properties such as the threshold voltage in a controlled manner, we followed a different integration procedure for PVP. Through a photografting process, CNTFETs were polymerized stepwise *in situ* with 4-vinylpyridine while the structural (with Raman spectroscopy) and electrical properties of CNTFETs were monitored. Figure 4(a) shows the transfer characteristics of an individual CNTFET during an *in situ* polymerization process. As can be seen, I_{on}/I_{off} increases significantly by almost four orders of magnitude (figure 4(b)). Moreover, a decreasing subthreshold swing and threshold voltage can be directly observed for the different polymerization times. Hence the same qualitative result was observed for spin-on passivation as well as passivation via *in situ* polymerization. Contact artifacts, like additional resistance at the CNT-metal interface due to the *in situ*

polymerization, can be excluded, since the ends of the CNTs are fully embedded in palladium. However, in contrast to the spin-on passivation, defects are induced into the CNTs. Raman spectroscopy revealed that CNT polymerization strongly impacts the quality of the CNTs. The D/G⁺ ratio, which gives a qualitative measure of the CNTs quality [56], increases by a factor of (4.8 ± 1.7) , implying a pronounced introduction of defects in the CNTs due to the covalent functionalization process. This implies that the CNTFETs' drain current decreases. Furthermore, up to a polymerization time of 30 min, no significant change in the I_{off} could be observed. This implies that this time is needed to establish a critical PVP density efficient enough to work as a passivation layer. In total, eight CNTFETs were analyzed. They all exhibit qualitatively the same trend. At a certain polymerization time, the I_{on}/I_{off} starts to increase. A comparison of the I_{on}/I_{off} for different devices can be found in the supplementary information. To confirm the correlation between a reduction in the doping concentration of CNTFETs with bundled CNTs and an increasing I_{on}/I_{off} ratio, we performed electrical transport simulations. The experimental data can be described by a superposition of the current-voltage characteristics of single CNTs and bundled CNTs. Single CNTs have a threshold voltage well below the maximum applied gate voltage and hence can be switched off within the possible bias region. In contrast, bundled CNTs have a much

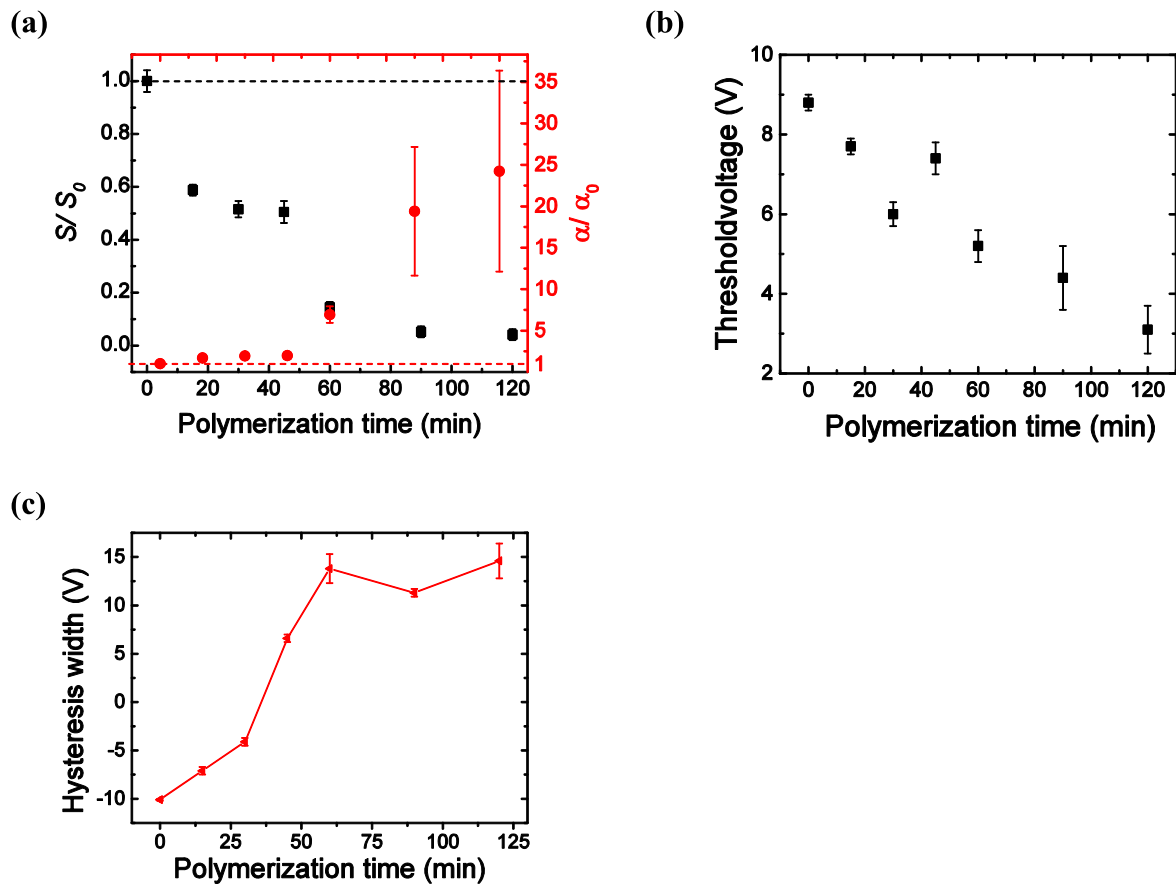


Figure 5. (a) Subthreshold swing S and gate efficiency parameter α as a function of polymerization time normalized to the pristine state. (b) Threshold voltage and (c) hysteresis width of CNTFETs upon polymerization.

higher threshold voltage, even for the same water-induced doping concentration. Thus, the total current of the multi-tube channel has a much lower $I_{\text{on}}/I_{\text{off}}$ ratio for the untreated channel, as shown in figure 4(c). For these simulations, we have assumed that 1 out of 6 tubes is part of a CNT bundle. Therefore, even a relatively low number of CNT bundles can already significantly affect the transistor behavior under ambient conditions. As the duration of the polymerization increases, the effective doping concentration decreases, which lowers the threshold voltage significantly, especially for the bundled CNTs, thus increasing the $I_{\text{on}}/I_{\text{off}}$ ratio accordingly, as shown in figure 4(d). However, I_{on} decreases as well, since the potential barriers at the contacts become more effective for lower doping concentrations, thereby reducing the current in the on-state.

The effectiveness of the *in situ* polymerization can be monitored as a change in the subthreshold swing or gate efficiency parameter over the polymerization time (figure 5(a)). Similar to the $I_{\text{on}}/I_{\text{off}}$ behavior, the gate efficiency increases strongly after 45 min of polymerization up to a factor of 24 compared to the original state. The final subthreshold swing was drastically reduced to 4% of the state before *in situ* passivation. These improvements are due to the higher permittivity of PVP compared to air, leading to increased gate efficiency. The coverage of the CNTs with PVP increases continuously, thereby increasing the effective passivation, which leads to a continual increase in gate

efficiency until full CNT coverage is reached. Not only the $I_{\text{on}}/I_{\text{off}}$ and subthreshold swing but also other FOMs, like the hysteresis width and the threshold voltage, changed with increasing polymerization time, due to the continuously increasing effectiveness of the passivation layer. As can be seen figure 5(b), the desired threshold voltage for CNTFET-based circuits can properly be adjusted in a range between 9 and 3 V for this individual device. Additionally, the hysteresis width changes upon *in situ* passivation (figure 5(c)), due to the diminished influence of the ambient (i.e., water or oxygen molecules). The hysteresis width strongly changes its magnitude and direction.

Since the direction or sign of the hysteresis changes upon *in situ* polymerization, a different process or charge trap type becomes more dominant, like mobile ions in the oxide or interface states. Before the *in situ* polymerization process, the typical counterclockwise hysteresis was observed as is usually found for such device configurations [57]. Afterwards, the hysteresis was clockwise. The very origin of this phenomenon is currently discussed in the literature [25, 58]. However, by properly adjusting the polymerization time, the overall hysteresis can be minimized. Transfer characteristic loops measured at certain polymerization times can be found in the supplementary information figure S8. In contrast to the spin-on passivation approach, the passivation approach via *in situ* polymerization facilitates adjusting CNTFET properties in a very controllable manner. The $I_{\text{on}}/I_{\text{off}}$ and threshold

voltage can be tuned in a broad range, and the hysteresis width can be minimized. Furthermore, this passivation approach allows the dynamics of the polymerization process to be studied and gives insights into charge traps relevant for CNTFETs.

4. Conclusions

In summary, we passivated CNTFETs with PVP via a spin-on polymerization approach and an *in situ* polymerization approach. Our results show that the high off currents of wet-processed short channel CNTFETs are not only due to parasitic metallic CNTs but also due to CNT bundles. This was confirmed by electrical transport simulations. A proper device passivation reduces the impact of CNT bundles on the electrical properties, since the gate coupling to the CNT ensemble is increased and the influence of oxygen-induced p-type doping is lowered. Thus, in our study, the on–off current ratio increased by up to five orders of magnitude and the sub-threshold swing decreased by one order of magnitude. This tremendous increase is beneficial, for example, for the HF performance of CNTFETs for digital and analog [59] applications. The *in situ* polymerization approach also enables the threshold voltage and the hysteresis width of the devices to be tuned. Hysteresis can even be reduced until it almost vanishes. This passivation approach allows devices based on wet-processed CNTs with improved performance to be fabricated using scalable technologies.

Acknowledgments

This work is supported by the German Research Foundation (DFG) through the Cluster of Excellence ‘Center for Advancing Electronics Dresden’ (EXC1056/1). We thank Michael Rennau from TU Chemnitz for CV measurements and Almut Pöhl as well as Dr Darius Pohl for TEM lamella preparation and TEM investigations.

ORCID iDs

Martin Hartmann  <https://orcid.org/0000-0002-4102-897X>

References

- [1] Cao Y, Brady G J, Gui H, Rutherglen C, Arnold M S and Zhou C 2016 *ACS Nano* **10** 6782–90
- [2] Dürkop T, Getty S A, Cobas E and Fuhrer M S 2004 *Nano Lett.* **4** 35–9
- [3] Baumgardner J E, Pesetski A A, Murduck J M, Przybysz J X, Adam J D and Zhang H 2007 *Appl. Phys. Lett.* **91** 52107
- [4] Mothes S, Claus M and Schroter M 2015 *IEEE Trans. Nanotechnol.* **14** 372–8
- [5] Schroter M, Claus M, Sakalas P, Haferlach M and Wang D 2013 *IEEE J. Electron Devices Soc.* **1** 9–20
- [6] Brady G J, Way A J, Safron N S, Evensen H T, Gopalan P and Arnold M S 2016 *Sci. Adv.* **2** e1601240
- [7] Qiu C, Zhang Z, Xiao M, Yang Y, Zhong D and Peng L-M 2017 *Science* **355** 271–6
- [8] Artukovic E, Kaempgen M, Hecht D S, Roth S and Gruner G 2005 *Nano Lett.* **5** 757–60
- [9] Schiessl S P, Fröhlich N, Held M, Gannott F, Schweiger M, Forster M, Scherf U and Zaumseil J 2015 *ACS Appl. Mater. Interfaces* **7** 682–9
- [10] Han X, Janzen D C, Vaillancourt J and Lu X 2007 *Micro Nano Lett.* **2** 96
- [11] Yamamoto K, Akita S and Nakayama Y 1996 *Japan. J. Appl. Phys.* **35** L917–8
- [12] Yamamoto K, Akita S and Nakayama Y 1996 *Appl. Phys. Lett.* **35** L917–8
- [13] Sarker B K, Shekhar S and Khondaker S I 2011 *ACS Nano* **5** 6297–305
- [14] Hennrich F, Li W, Fischer R, Lebedkin S, Krupke R and Kappes M M 2016 *ACS Nano* **10** 1888–95
- [15] Nish A, Hwang J-Y, Doig J and Nicholas R J 2007 *Nat. Nanotechnol.* **2** 640–6
- [16] Hwang J-Y, Nish A, Doig J, Douven S, Chen C-W, Chen L-C and Nicholas R J 2008 *J. Am. Chem. Soc.* **130** 3543–53
- [17] Jakubka F, Schießl S P, Martin S, Englert J M, Hauke F, Hirsch A and Zaumseil J 2012 *ACS Macro Lett.* **1** 815–9
- [18] Shea M J, Mehlenbacher R D, Zanni M T and Arnold M S 2014 *J. Phys. Chem. Lett.* **5** 3742–9
- [19] Graf A, Zakharko Y, Schießl S P, Backes C, Pfohl M, Flavel B S and Zaumseil J 2016 *Carbon* **105** 593–9
- [20] Lee C W, Weng C-H, Wei L, Chen Y, Chan-Park M B, Tsai C-H, Leou K-C, Poa C H P, Wang J and Li L-J 2008 *J. Phys. Chem. C* **112** 12089–91
- [21] Toader M, Schubel R, Hartmann M, Scharfenberg L, Jordan R, Mertig M, Schulz S E, Gessner T and Hermann S 2016 *Chem. Phys. Lett.* **661** 1–5
- [22] Cao Y, Che Y, Gui H, Cao X and Zhou C 2016 *Nano Res.* **9** 363–71
- [23] Hu Y et al 2015 *Nat. Commun.* **6** 6099
- [24] Collins P G 2000 *Science* **287** 1801–4
- [25] Tittmann-Otto J, Hermann S, Kalbacova J, Hartmann M, Toader M, Rodriguez R D, Schulz S E, Zahn D R T and Gessner T 2016 *J. Appl. Phys.* **119** 124509
- [26] Tittmann J, Hermann S, Schulz S E, Pacheco-Sanchez A, Claus M and Schroter M 2014 *Proc. 2014 IEEE/ACM Int. Symp. on Nanoscale Architectures* pp 137–8
- [27] Haferlach M, Pacheco A, Sakalas P, Alexandru M, Hermann S, Nardmann T, Schroter M and Claus M 2016 *IEEE Trans. Nanotechnol.* **15** 619–26
- [28] Kang D, Park N, Ko J-H, Bae E and Park W 2005 *Nanotechnology* **16** 1048–52
- [29] Derycke V, Martel R, Appenzeller J and Avouris P 2002 *Appl. Phys. Lett.* **80** 2773
- [30] Bisri S Z, Derenskyi V, Gomulya W, Salazar-Rios J M, Fritsch M, Fröhlich N, Jung S, Allard S, Scherf U and Loi M A 2016 *Adv. Electron. Mater.* **2** 1500222
- [31] Shim M, Javey A, Shi Kam N and Dai H 2001 *J. Am. Chem. Soc.* **123** 11512–3
- [32] Bockrath M, Hone J, Zettl A, McEuen P L, Rinzler A G and Smalley R E 2000 *Phys. Rev. B* **61** R10606–8
- [33] Martel R, Derycke V, Lavoie C, Appenzeller J, Chan K K, Tersoff J and Avouris P 2001 *Phys. Rev. Lett.* **87** 256805
- [34] Wang C, Ryu K, Badmaev A, Zhang J and Zhou C 2011 *ACS Nano* **5** 1147–53
- [35] Lin Y-M, Appenzeller J, Knoch J and Avouris P 2005 *IEEE Trans. Nanotechnol.* **4** 481–9
- [36] Mizutani T, Iwatsuki S, Ohno Y and Kishimoto S 2005 *Japan. J. Appl. Phys.* **44** 1599–602

- [37] Kaminishi D, Ozaki H, Ohno Y, Maehashi K, Inoue K, Matsumoto Yasuhiro Seri K, Masuda A and Matsumura H 2005 *Appl. Phys. Lett.* **86** 113115
- [38] Kim W, Javey A, Vermesh O, Wang Q, Li Y and Dai H 2003 *Nano Lett.* **3** 193–8
- [39] Shimauchi H, Ohno Y, Kishimoto S and Mizutani T 2006 *Japan. J. Appl. Phys.* **45** 5501–3
- [40] Rispal L, Tschischke T, Yang H and Schwalke U 2008 *Japan. J. Appl. Phys.* **47** 3287–32891
- [41] Bradley K, Cumings J, Star A, Gabriel J-C P and Grüner G 2003 *Nano Lett.* **3** 639–41
- [42] Ha T-J, Kiriya D, Chen K and Javey A 2014 *ACS Appl. Mater. Interfaces* **6** 8441–6
- [43] Lefebvre J, Ding J, Li Z, Cheng F, Du N and Malenfant P R L 2015 *Appl. Phys. Lett.* **107** 243301
- [44] Lou X, Detrembleur C, Pagnouille C, Jérôme R, Bocharova V, Kiriya A and Stamm M 2004 *Adv. Mater.* **16** 2123–7
- [45] Javey A, Guo J, Wang Q, Lundstrom M and Dai H 2003 *Nature* **424** 654–7
- [46] Zhang Y, Franklin N W, Chen R J and Dai H 2000 *Chem. Phys. Lett.* **331** 35–41
- [47] Chen Z, Appenzeller J, Knoch J, Lin Y-M and Avouris P 2005 *Nano Lett.* **5** 1497–502
- [48] NanoIntegris (Accessed: 2017) <http://nanointegris.com/en/semi-conducting>
- [49] Steenackers M, Kuller A, Stoycheva S, Grunze M and Jordan R 2009 *Langmuir* **25** 2225–31
- [50] Estrada D, Dutta S, Liao A and Pop E 2010 *Nanotechnology* **21** 85702
- [51] Claus M, Mothes S, Blawid S and Schröter M 2014 *J. Comput. Electron.* **13** 689–700
- [52] Léonard F 2006 *Nanotechnology* **17** 2381–5
- [53] Appenzeller J, Knoch J, Martel R, Derycke V, Wind S and Avouris P 2005 *Appl. Phys. Lett.* **86** 285–8
- [54] Rosenblatt S, Yaish Y, Park J, Gore J, Sazonova V and McEuen P L 2002 *Nano Lett.* **2** 869–72
- [55] Siddons G, Merchin D, Back J, Jeong J and Shim M 2004 *Nano Lett.* **4** 927–31
- [56] Kalbac M, Hsieh Y-P, Farhat H, Kavan L, Hofmann M, Kong J and Dresselhaus M S 2010 *Nano Lett.* **10** 4619–26
- [57] Ong H G, Cheah J W, Zou X, Li B, Cao X H, Tantang H, Li L-J, Zhang H, Han G C and Wang J 2011 *J. Phys. D: Appl. Phys.* **44** 285301
- [58] Toader M, Hermann S, Scharfenberg L, Hartmann M, Mertig M, Schulz S E and Gessner T 2016 *J. Phys. Chem. C* **120** 10020–6
- [59] Nougaret L, Happy H, Dambrine G, Derycke V, Bourgoin J-P, Green A A and Hersam M C 2009 *Appl. Phys. Lett.* **94** 243505